Microchimica Acta (2021) 188: 423
https://doi.org/10.1007/s00604-021-05080-w

ORIGINAL PAPER

Multicolor diagnosis of salivary alkaline phosphatase triggered by silver-coated gold nanobipyramids

Eslam Hafez[1,2,3] · Byeong-Seok Moon[1] · Samy M. Shaban[1,2,3] · Do-Gi Pyun[4] · Dong-Hwan Kim[1,2]

Received: 19 October 2021 / Accepted: 24 October 2021 / Published online: 18 November 2021
© The Author(s), under exclusive licence to Springer-Verlag GmbH Austria, part of Springer Nature 2021

Abstract

Alkaline phosphatase (ALP) is one of the most versatile biomarkers for early detection of several diseases, such as oral carcinomas and periodontitis; therefore, great efforts have been dedicated for developing an ALP biosensor. Multicolor detection of ALP in saliva is ideal for a point-of-care diagnosis; however, this approach is very challenging since spectral responses over wavelengths of several tens of nanometers have thus far remained difficult to achieve. In this work, a colorimetric biosensor for ALP assay has been developed based on ALP affinity to dephosphorylate glucose phosphate into glucose, which has the affinity to deposit Ag nanoshells onto Au nanobipyramids with a multicolor response. This approach provides a blue shift of localized surface plasmon resonance (LSPR) as large as 190 nm corresponding to distinctive color changes, from yellowish brown to red based on the thickness of the formed Ag shell around the Au nanobipyramids. The change in the LSPR has been conducted for highly sensitive quantitative bioassay of ALP with a detectable multicolor change with linear dynamic range of 0.1–20 U/L and low limit of detection (LOD) of 0.085 U/L. Furthermore, the developed multicolor ALP biosensor exhibits high selectivity with high recovery of 98.6% demonstrating its reliability and suitability for a point-of-care diagnosis.

Keywords Gold nanobipyramids · Core–shell nanoparticles · Multicolor biosensor · Surface plasmon resonance · Alkaline phosphatase · Salivary diagnosis · Point-of-care diagnosis

Introduction

Rapid detection of diseases is a key to its forecast outcome and effective disease management. Early diagnosis requires an easy and non-invasive method, which makes the diagnosis by saliva more convenient than the diagnosis by blood or tissue [1]. Among the target diseases of salivary diagnosis, periodontal diseases (i.e., gingivitis and periodontitis), which gradually destroy the teeth-supporting structures, including both soft and hard tissues, eventually result in tooth loss. The alkaline phosphatase (ALP) enzyme is one of the biomarkers typically used to diagnose periodontal diseases, owing to its ability to indicate both inflammation and destruction of periodontal tissues. ALP can be found in saliva via three different routes, namely, salivary secretion, gingival crevicular fluid generated by tissue degradation, and bacterial cells that are responsible for periodontal diseases [2]. Previous studies exploiting ALP in saliva as a diagnostic biomarker have successfully correlated with the degree of periodontal disease [3, 4]. For ALP assay, diverse strategies have been demonstrated, including colorimetric biosensors [5–9], fluorometric biosensors [10–13], Raman scattering spectroscopy [14–17], capillary electrophoresis [18–20], and electrochemical biosensors [21–23]. Among them, colorimetric ALP biosensors detect the chromogenic differences of phosphate substrates and its dephosphorylated products to provide simple and fast quantitative results using instrumentation of reduced complexity, which renders them suitable candidates for a point-of-care diagnosis through color changes over a wide range of analyte concentrations [24, 25]. ALP possesses the catalytic activity to dephosphorylate various phosphate substrates, such as *p*-nitrophenyl phosphate, disodium phenyl phosphate, and ascorbic acid

✉ Dong-Hwan Kim
dhkim1@skku.edu

1 School of Chemical Engineering, Sungkyunkwan University, Suwon 16419, Republic of Korea

2 Biomedical Institute for Convergence at SKKU (BICS), Sungkyunkwan University, Suwon 16419, Republic of Korea

3 Petrochemical Department, Egyptian Petroleum Research Institute, Cairo, Egypt

4 Biomedical Polymer R&D Institute, T&L Co., Ltd, Anseong 17554, South Korea

(AA) phosphate [26–31]. AA phosphate has been intensively studied as a substrate for the ALP assay [8, 32–35]; however, AA and AA phosphate have been used recently in periodontal therapy in the form of coatings and/or gel forms to enhance the osseointegration of dental implants and improve post-surgical periodontal healing, so their concentration changes in saliva [36–39], resulting in false positive results. So, searching for an alternative phosphate substrate that develops a multicolorimetric response for ALP enzyme is still highly needed.

Here, we developed a highly sensitive multicolor ALP biosensor based on its catalytic affinity to convert the α-D-glucose 1-phosphate (first time to use glucose phosphate as substrate to detect the ALP enzyme) into glucose. The released glucose has been involved in generating a multicolor response as function of ALP concentration as provided in Scheme 1. We successfully used glucose to induce a homogenous overgrowth of AgNPs on the surface of Au bipyramids with the assistance of a mixed surfactants consisting of CTAB and Tween 20. The released glucose induced a blue shift of the LSPR from 740 to 550 nm with distinctive color changes, from yellowish brown, to green, blue, purple, and red, as the ALP concentration increases from 0 to 50 U/L with low limit of detection of 0.1 U/L. The developed biosensor also shows great selectivity against various biomolecules which commonly exist in saliva. The salivary diagnosis of ALP was conducted using a standard addition method with a high recovery rate of 98.6%. It is anticipated that the multicolor ALP biosensor developed in this study will pave the way for practical salivary diagnosis of periodontal diseases and will be of guidance for the development of highly sensitive salivary biosensors toward other target diseases.

Experimental section

Synthesis and purification of gold nanobipyramids (AuNBPs)

AuNBPs were synthesized via a seed-mediated growth method [40]. The seed solution was synthesized by injecting $NaBH_4$ (0.01 M, 0.6 mL) into a solution containing $HAuCl_4$ (0.01 M, 0.5 mL), trisodium citrate (0.01 M, 1 mL), and water (38.5 mL) under vigorous stirring. The seed solution was aged in the dark for 5 h before being used. Next, the as-prepared seed solution (5 mL) was injected into the solution containing $HAuCl_4$ (0.01 M, 10 mL), $AgNO_3$ (0.01 M,

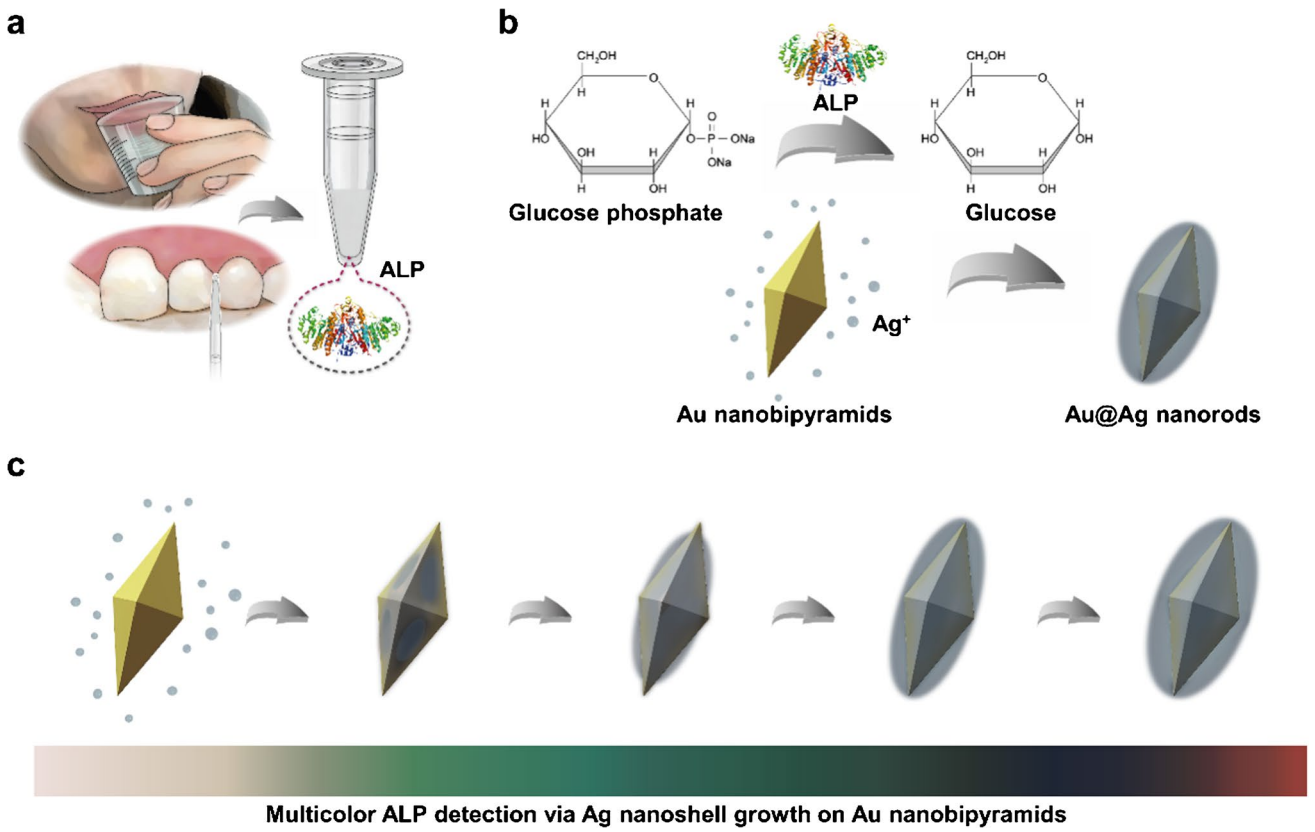

Scheme 1 Schematic illustration of the multicolor ALP biosensor based on the compositional and morphological changes of AuNBPs

2 mL), hydrochloric acid (HCl, 1 M, 4 mL), AA (0.1 M, 1.6 mL), and CTAB (0.1 M, 200 mL) with gentle shaking for 2 min, until the color of the mixed solution became purple. The solution was then kept in a water bath overnight at 30 °C.

The resulting solution comprises spherical, rod-like, and bipyramidal gold nanoparticles, exhibiting two distinctive LSPR peaks at 550 and 750 nm, as shown in Fig. S1 (Supporting Information). To improve the monodispersity of AuNBPs, further purification was performed following work presented elsewhere [41]. Firstly, the prepared AuNBP solution was centrifuged at 10,000 rpm for 10 min and redispersed in a CTAC solution (0.08 M, 150 mL). Subsequently, $AgNO_3$ (0.01 M, 40 mL) and AA (0.1 M, 20 mL) were added, and the solution was then kept in a water bath (65 °C, 4 h) to form Au@Ag core–shell nanowires (Fig. S2). The nanowires form as a result of the selective growth of silver shells onto the favorable facets of AuNBPs. To separate the nanowires, the solution was centrifuged at 6000 rpm for 10 min, and the supernatant was discarded. The precipitate was redispersed in a CTAB solution (0.05 M, 150 mL) and kept at room temperature for 5 h for the precipitation of the nanowires, followed by redispersion in water (100 mL). The Au@Ag core–shell nanowires show LSPR peaks at 600 and 770 nm, which originate from the transverse and longitudinal modes, respectively. Lastly, all the Ag nanoshells were etched by adding $NH_3{\cdot}H_2O$ (28%, 10 mL) and H_2O_2 (5%, 1 mL); the solution was left to rest for 4 h. The Ag nanoshells were oxidized and precipitated as AgCl. The supernatant, which contains AuNBPs, which show LSPR peaks at 550 and 740 nm originate from the transverse and longitudinal modes, respectively, was centrifuged at 8000 rpm for 10 min and redispersed in a solution containing CTAB and Tween 20 for further use.

Colorimetric response upon glucose

We firstly examined the colorimetric responses of our ALP biosensor toward glucose, which is produced from glucose phosphate by the catalytic activity of ALP, to validate the deposition of Ag^+ ions on the AuNBPs. The AuNBP solution (750 µL), $AgNO_3$ (500 µL, 10 mM), and $NH_3{\cdot}H_2O$ (100 µL, 10 mM) were mixed in a glass vial. A glucose solution (100 µL) of various concentrations was then added to the prepared mixture and kept at 50 °C for 2 min. The colorimetric response was monitored using an UV–Vis spectrometer (JASCO V 770, Japan) and observed by the naked eye.

Multicolor detection of ALP

One hundred microliters of a Tris-base solution (10 mM, pH 9.8) containing ALP of various concentrations (0.1–50 U/L) was mixed with 100 µL of a α-D-glucose 1-phosphate disodium salt hydrate aqueous solution (1.5 mM), and the resulting solution was incubated for 45 min at 37 °C in a water bath to produce glucose. After the incubation, a mixture of AuNBPs (750 µL), $AgNO_3$ (500 µL, 10 mM), and $NH_3{\cdot}H_2O$ (100 µL, 10 mM) was added to the previous solution, which in the meantime had been heated to 50 °C. The colorimetric detection in absorbance and color was evaluated after 2-min incubation time with an UV–Vis spectrometer and with the naked eye, respectively.

Selectivity test for the ALP assay

To test the selectivity of the ALP assay, various interfering species (amylase, lipase, mucins, BSA, MMP-9, and lysozyme), which are commonly present in saliva, were investigated both individually and combined with ALP under the same conditions described in multicolor detection of ALP section.

Salivary diagnosis of ALP

Saliva samples containing ALP of unknown concentration were directly collected from the mouth of a volunteer through a soft plastic catheter after a 3-min mouth cleansing, prior to breakfast. The saliva that was collected during the first 10 s was discarded; saliva samples of 5 mL were then collected in sterile test tubes. After centrifugation at 1000 rpm for 15 min, the saliva samples were stored at − 80 °C until analysis [41].

The collected saliva was diluted 10 times using a Tris-base solution (10 mM, pH 9.5) before the ALP assay, using the same procedures described in multicolor detection of ALP section. The ALP assay was conducted via a standard addition method using standard ALP solutions to get the concentration of ALP in saliva. The recovery rate for our sensor was done by adding standard ALP concentrations of 0, 0.5, 3, and 5 U/L. Firstly, 100 µL of the diluted saliva was examined, and the standard ALP solutions were added to the diluted saliva solution. One hundred microliters of the resulting mixture was then examined to evaluate the recovery rate. The recovery rate was calculated according to:

$$\text{Recovery rate (\%)} = \frac{\text{Measured concentration}}{\text{Added concentration}} \times 100$$

Results and discussion

Validation of the AuNBP-based multicolor biosensor

AuNBPs exhibit an intense absorption peak at 740 nm corresponding to the LSPR longitudinal mode (Fig. 1a), which is highly sensitive to the aspect ratio of the nanostructures.

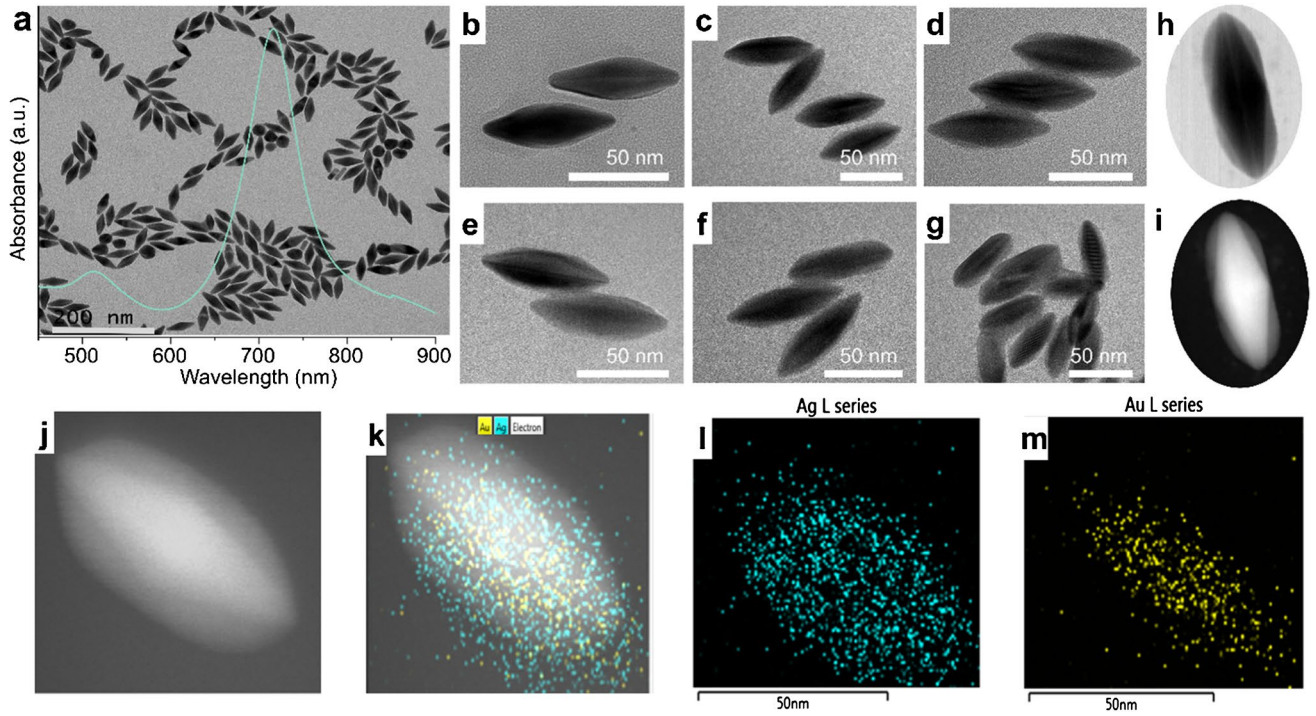

Fig. 1 (**a**–**g**) TEM images of the monodisperse AuNBPs after reacting with glucose with concentrations of 0 (**a**), 10 (**b**), 20 (**c**), 30 (**d**), 40 (**e**), 50 (**f**), and 60 (**g**) μM. The AuNBP absorption spectrum is illustrated in the inset of (**a**). (**h**, **i**) TEM (**h**) and HAADF-STEM (**i**) images of the AuNBPs@Ag core–shell nanorod synthesized using 60 μM glucose. (**j**–**m**) Elemental mapping of the AuNBPs@Ag core–shell nanorod synthesized using 70 μM glucose

Therefore, to attain high sensitivity of the ALP assay, we exploited the longitudinal mode of the AuNBPs by changing the nanoparticle morphology from narrow bipyramidal to thick rod-like upon Ag nanoshell deposition. In this ALP assay, glucose is released from added glucose phosphate, which exists in negligible quantities in saliva, by ALP catalytic hydrolysis, as depicted in Scheme 1. Glucose reduces Ag ions to precipitate Ag nanoshells onto AuNBPs, resulting in both compositional and morphological changes that induce huge LSPR responses for the ALP assay with distinctive multicolor response. To achieve the best performance for the proposed multicolor biosensor with high degree of colorimetric responses, we firstly prepared monodispersed AuNBPs via purification process, as described before. Upon increasing the glucose concentration, a large blue shift of the absorption peak from 740 to 550 nm can be observed and is attributed to the increased precipitation of Ag nanoshells onto AuNBPs (Fig. 1b–g) with distinctive color changes (Fig. 2c). The tonality and the color sensitivity depend on the thickness and homogeneity of the deposited AgNPs on the surface of AuNBPs and will be explained briefly later. The presence of the Ag nanoshell was confirmed with a high-angle annular dark-field scanning transmission electron microscope (HAADF-STEM) (Fig. 1h, i), element mapping (j–m), and elemental analysis (Fig. S3) which clearly show that the nanostructures are composed of an AuNBP core surrounded by an Ag nanoshell. It is notable that the length of the AuNBPs does not change before and after Ag nanoshell deposition, while the thickness of AuNBPs is increased after the Ag deposition, implying significant changes in the aspect ratio accompanied with a large blue shift of the LSPR longitudinal mode. The reason behind the observed Ag nanoshell deposition is to reduce the surface energy of the high-index facets of AuNBPs [37–39].

Multicolor biosensor response upon glucose concentration variations

For ultra-sensitivity of longitudinal LSPR to glucose response, the developed assaying method needs to be optimized, where some parameters were investigated like solution pH and concentration of the shape-directing agents: $AgNO_3$ and the surfactant ratio. The proposed sensing mechanism depends on the glucose affinity to reduce the shape-directing agents $AgNO_3$ to AgNPs on the surface of the bare AuNBPs with inducing change in the longitudinal LSPR; therefore, the pH of the solution is significantly controlling the sensor sensitivity because glucose is a pH-dependent sugar-reducing agent. Increasing the solution pH promotes the reduction affinity of the sugar-reducing

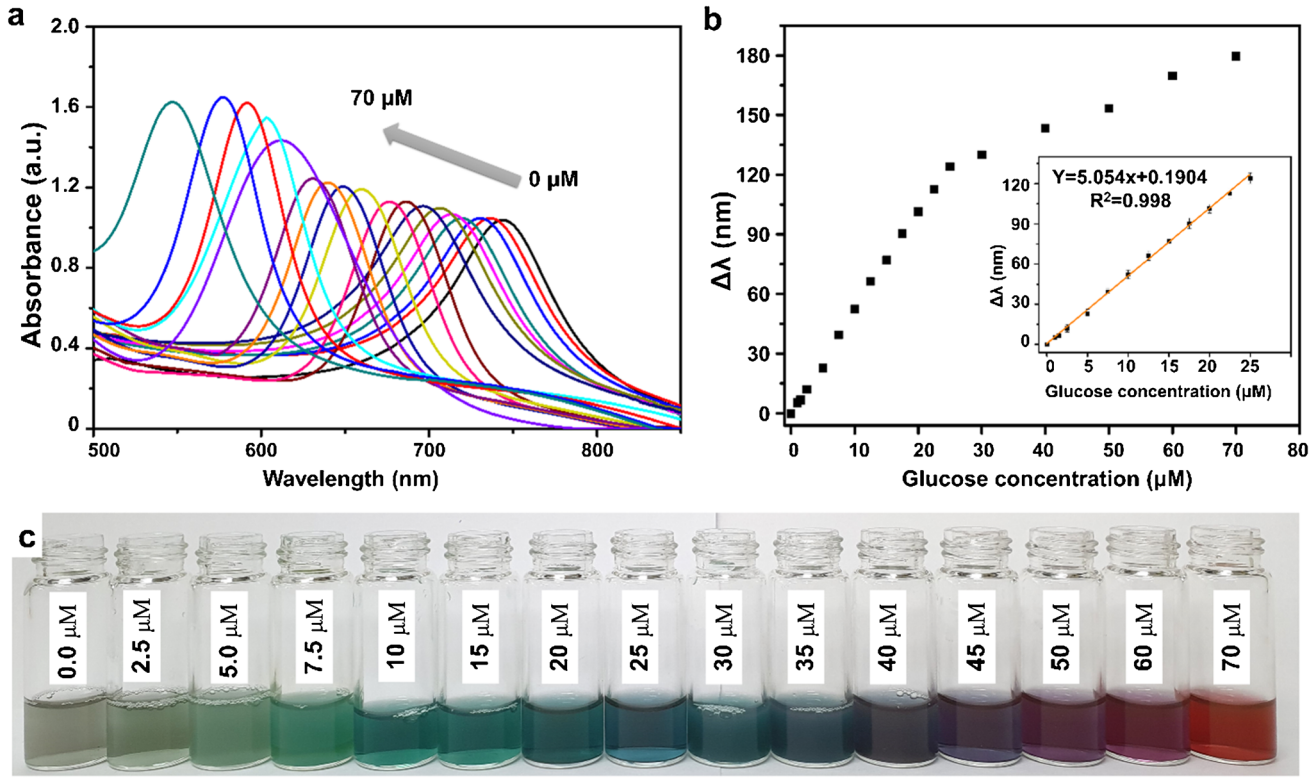

Fig. 2 (**a**) UV–Vis spectra of the multicolor biosensor as a function of glucose concentration. (**b**) Standard plotting of the amplitude of the blue shift of a LSPR peak ($\Delta\lambda$) as a function of the glucose concentration. The inset illustrates the linear calibration plot. (**c**) Multicolor changes of AuNBPs upon Ag nanoshell deposition as a function of the glucose concentration (ranging from 0 to 70 µM). These experiments were conducted using 750 µL of the as-prepared AuNBP solution, 500 µL of $AgNO_3$ (10 mM), 100 µL of NH_4OH (0.1 mM), and 100 µL of glucose with various concentrations

agent (glucose) and enhances the change in the longitudinal LSPR with maximum $\Delta\lambda$ shift at solution pH 10 and 11 (Fig. S4a, Supporting Information). However the solution pH = 11 induces some direct reduction for $AgNO_3$ solution into AgNPs away from the surface of bare AuNBPs which make a hue in the final color (because of color mixing of AgNPs alone in solution with color of Ag@AuNBPs). Hence, the pH = 10 was chosen as the optimum pH that promotes maximum blue shift of LSPR with best color resolution (Fig. S4a, Supporting Information).

The concentration of $AgNO_3$ was optimized for high sensitivity with maximum LSPR change (Fig. S4b, Supporting Information). Increasing the concentration of $AgNO_3$, the amount of the deposited AgNPs on AuNBP surface increases with maximum ($\Delta\lambda$) at concentration of 10 mM (Fig. S4b, Supporting Information). At $AgNO_3$ concentration higher than 10 mM of $AgNO_3$, the $\Delta\lambda$ decreases again with bad tunable color transition because of self-growth of AgNPs in solution beside overgrowth on the side surface of AuNBPs, which matches with another study [42], thus promoting anisotropic overgrowth of Ag on the bare AuNBPs [43]. So, 10 mM of $AgNO_3$ was used as the optimum concentration (Fig. S4b, Supporting Information).

Using a surfactant to control the homogenous growth of Ag on the Au surface was essential. We successfully provided a binary mixture of surfactants consisting of CTAB (2 mM) and Tween 20 of 0.25 mM as optimum ratio that achieved maximum LSPR shift with the best color response (Fig. S4c, Supporting Information). Hence, our optimum conditions are pH 10, $AgNO_3$ 10 mM, and 2:0.25 mM CTAB:Tween 20.

After sensor optimization, we examined the colorimetric response of the multicolor biosensor as a function of glucose concentrations from 0 to 70 µM via an UV–Vis spectrometer (Fig. 2a). Continuous blue shifts and an enhanced intensity of the absorption peak are observed in the range from 740 to 550 nm, resulting in distinctive color changes (Fig. 2c) as function of increase glucose concentration. Both the spectral shift and the intensity enhancement are attributed to changes in the dielectric functions and aspect ratio, which are induced by the formation of the Ag@Au bimetallic system [44–46]. The standard curve is plotted considering the amplitude of the blue shift, depending on the glucose concentration (Fig. 2b). The linear dynamic range of the

blue shift takes place from 0 to 25 μM (inset in Fig. 2b), so further experiments were conducted in this range with the aim of realizing a reliable and highly sensitive multicolor ALP biosensor.

ALP assay using the developed multicolor biosensor

As described in Scheme 1, the ALP assay is based on the catalytic ability of ALP to dephosphorylate glucose phosphate substrates into glucose, thus reducing Ag ions into Ag nanoshells on the AuNBP surface inducing a blue shift in the LSPR peak. Therefore, the operating condition between the ALP and the glucose substrate needs to be optimized. Hence, the glucose phosphate, incubation time, pH, and temperature need optimization for achieving high sensitivity. According to Gao et al. [47], the optimum pH and temperature for ALP are 9.8 and 37 °C, respectively. The concentration of the glucose phosphate was optimized as shown in the Fig. 3a, where the maximum LSPR blue shift was observed at concentration of 2 mM. The ALP was incubated with the glucose phosphate for different times and 45 min achieved the maximum LSPR blue shift (Fig. 3b).

Using the optimized conditions, various concentrations of the standard ALP solution were assayed via an UV–Vis spectrometer (Fig. 4a) as well as using the naked eye (Fig. 4c). As the ALP concentration increases from 0 to 50 U/L, a continuous blue shift of the LSPR peak was observed, implying the validity of the proposed detection strategy. The standard plot is plotted in terms of the blue shift amplitude as a function of the ALP concentration (Fig. 4b). The linear dynamic range was found to be from 0 to 20 U/L (inset in Fig. 4b), with low limit of detection of 0.085 U/L, as compared with previous works (Table 1) based on $3\sigma/m$, where σ is the standard deviation of the blank sample, and m is the slope of the calibration curve.

Selectivity test for the ALP assay

Saliva is secreted by salivary glands, and this fluid consists of water, electrolytes, enzymes, mucins, proteins, and immunoglobulins, so we investigated the interference of the developed multicolor biosensor with several biomolecules which commonly exist in saliva, including amylase, lipase, mucins, BSA, MMP-9, and lysozyme. We found that only ALP exhibits a large blue shift of the LSPR peak (Fig. 5a) and a distinctive color change (inset of Fig. 5a), whereas the other biomolecules showed negligible results. Next, the interference effects in the presence of ALP were investigated, and it was found that the peak shifts were almost identical (Fig. 5b), as clearly showed by the corresponding color changes (inset of Fig. 5b).

Salivary ALP diagnosis using the developed multicolor biosensor

Salivary ALP diagnosis was successfully demonstrated through our developed multicolor biosensor after dilution 10 times. The human salivary ALP ranges from 25

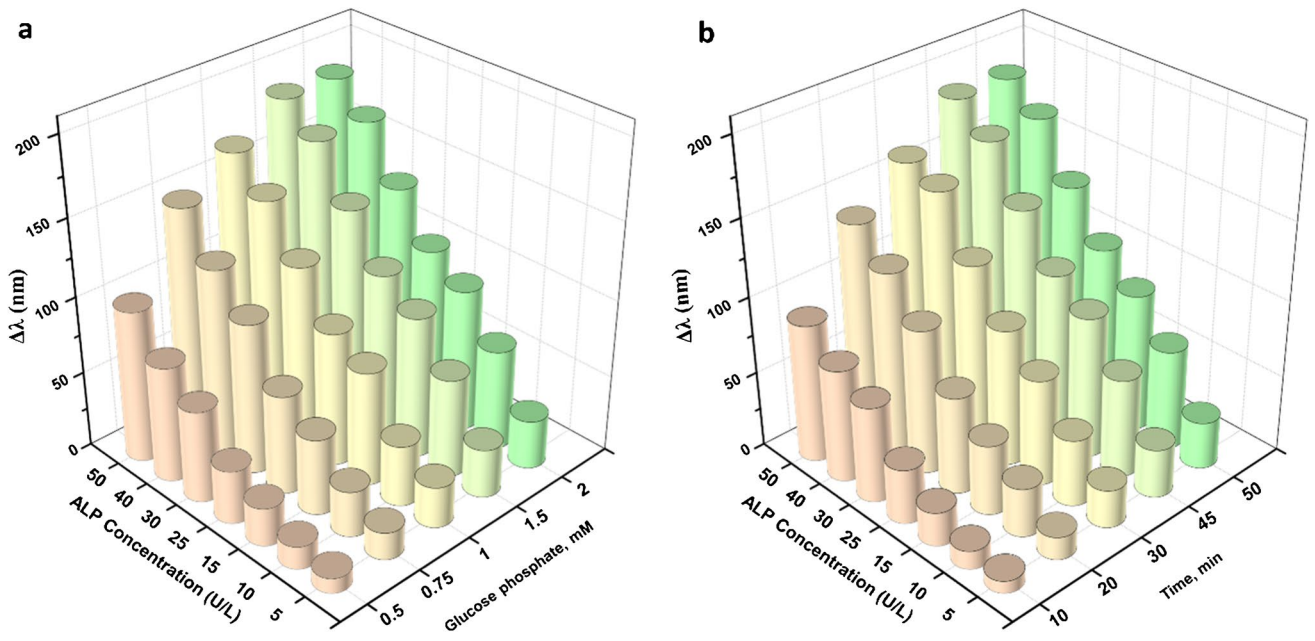

Fig. 3 3D plots illustrating the blue shift amplitude vs ALP concentration as a function of glucose phosphate concentration (**a**) and incubation time (**b**)

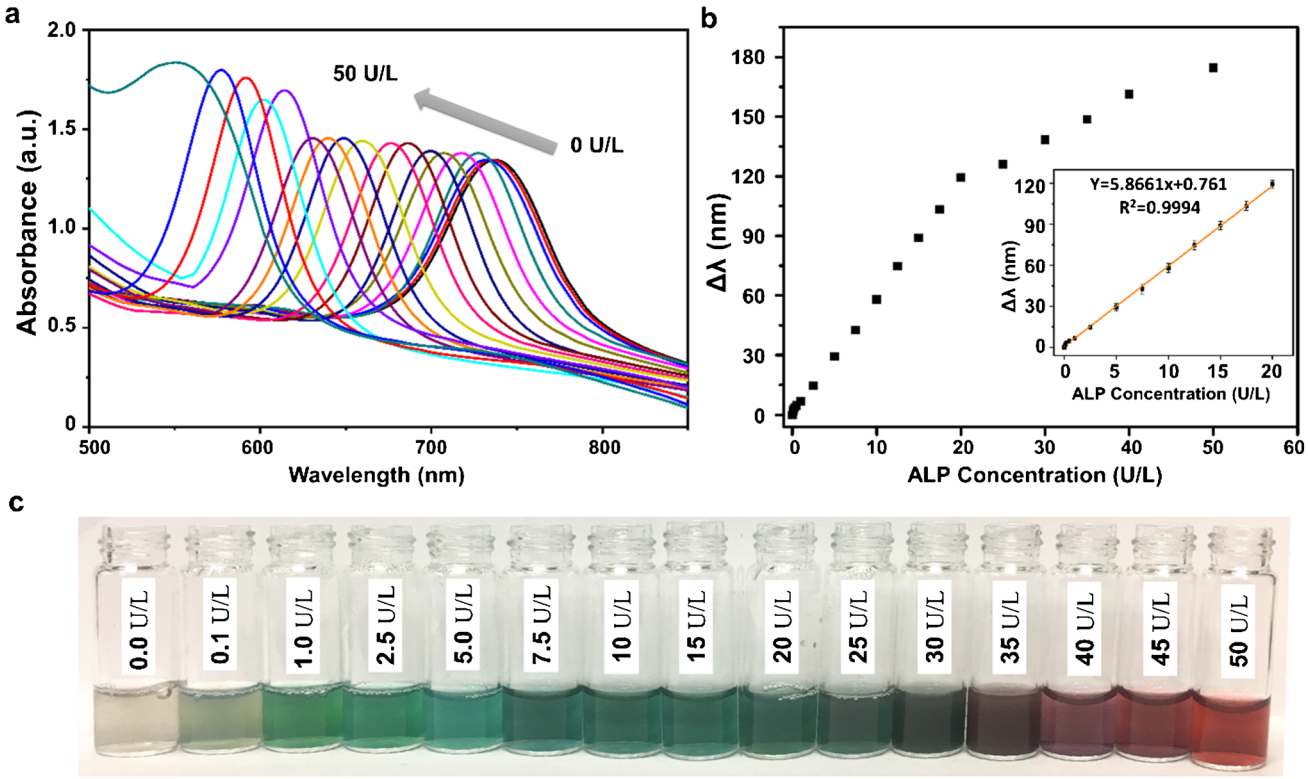

Fig. 4 (**a**) UV–Vis spectra of the multicolor biosensor as a function of the ALP concentration. (**b**) Standard plot in terms of the blue shift amplitude of the LSPR peak ($\Delta\lambda$) as a function of the ALP concentration, from 0 to 50 U/L. The inset illustrates the linear calibration plot. (**c**) Multicolor changes of the biosensor solution upon increasing the ALP concentration. The ALP concentrations used were 0, 0.1, 0.5, 1.25, 2.5, 5, 7.5, 12.5, 17.5, 20, 25, 30, 40, and 50 U/L. The ALP assay was conducted using 2 mM of glucose phosphate and a 45-min incubation time

Table 1 Performance comparison of ALP biosensors

Method	Linear range (U/L)	LOD (U/L)	Ref
Colorimetry	0.1–20	0.085	This work
Colorimetry	0–120	5.4	[5]
Colorimetry	1–34	0.19	[48]
Colorimetry	5–100	3.3	[7]
Colorimetry	0.2–20	0.1	[9]
Fluorescence	3.4–100	0.9	[49]
Fluorescence	0.2–30	0.2	[50]
Fluorescence	4.6–383.3	1.4	[51]
Fluorescence	0–150	0.15	[52]
Fluorescence	0–50	0.5	[53]
Electrochemistry	2–25	2	[54]

to 100 U/L, so diluting saliva 10 times will be included in our sensor linear range 0.1–20 U/L. Saliva was collected from a volunteer, according to the protocol described in the section collecting sample of saliva. The saliva sample with unknown ALP concentration was diluted 10 times using the Tris-base buffer. The ALP concentration in the 10% diluted saliva solution was then measured through our developed colorimetric biosensor using the standard addition method, as shown in Fig. 6a, b. The ALP concentration in the saliva before dilution amounted to be 46.6 U/L (Table 2). The recovery rates for each sample with standard addition of ALP ranged from 97.5 to 100.3%, with the corresponding relative standard deviations ranging from 3.91 to 4.75%, as shown in Table 2 and Figs. S6 and S7.

To verify the accuracy of our proposed method for assaying ALP enzyme in salivary diagnosis, we bought a standard ALP test kit for assaying ALP in saliva (alkaline phosphatase activity colorimetric assay kit (BioVision)). Three saliva samples were collected from different volunteers to validate our method with a standard enzymatic colorimetric test. The unknown ALP concentration in the three samples was determined using both our developed sensor and the standard ALP kit. The results showed good matching between our result and the standard kit result as described in Table S1 and Fig. S8 and S9 (Supporting Information). The results proved the potential applicability of our developed multicolor ALP biosensor for point-of-care diagnosis in dental clinics.

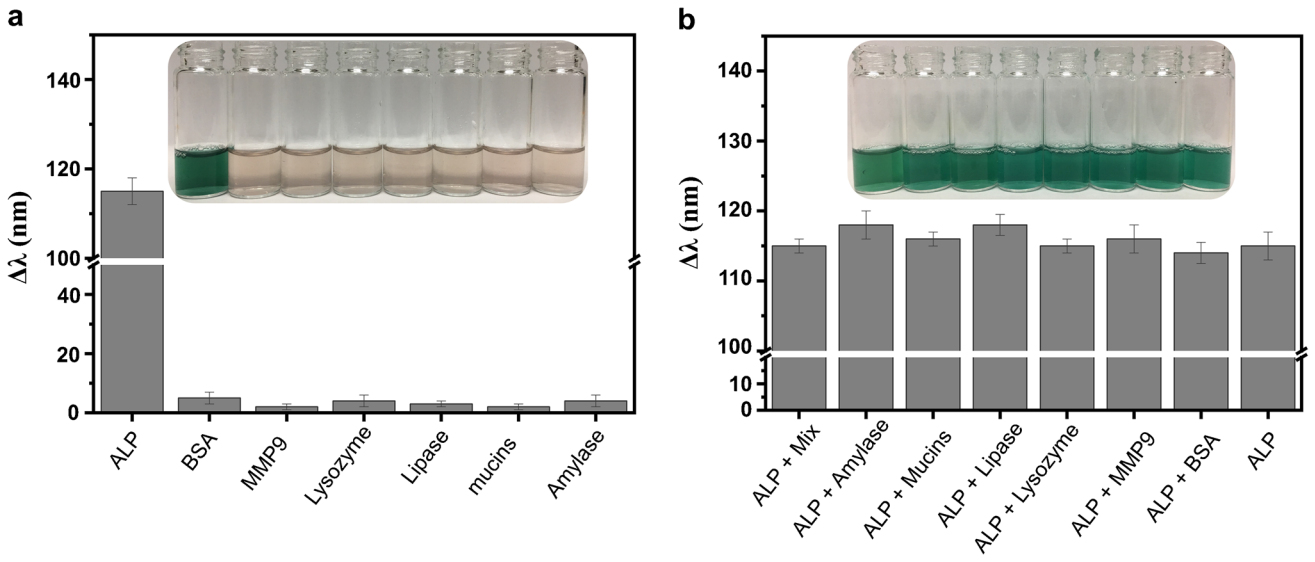

Fig. 5 (**a**) Selectivity test for the multicolor ALP biosensor combined with the most common biomolecules found in saliva. (**b**) Interference test of the multicolor ALP biosensor in the presence of the other biomolecules. The ALP concentration in the selectivity and interference test 20 U/L, whereas the concentrations of the interfering biomolecules were 100 μg/mL, 0.2 μg/mL, 150 μg/mL, 5 μg/mL, 2.5 mg/mL, and 100 μg/mL, for BSA, MMP-9, lysozyme, lipase, amylase, and mucins, respectively

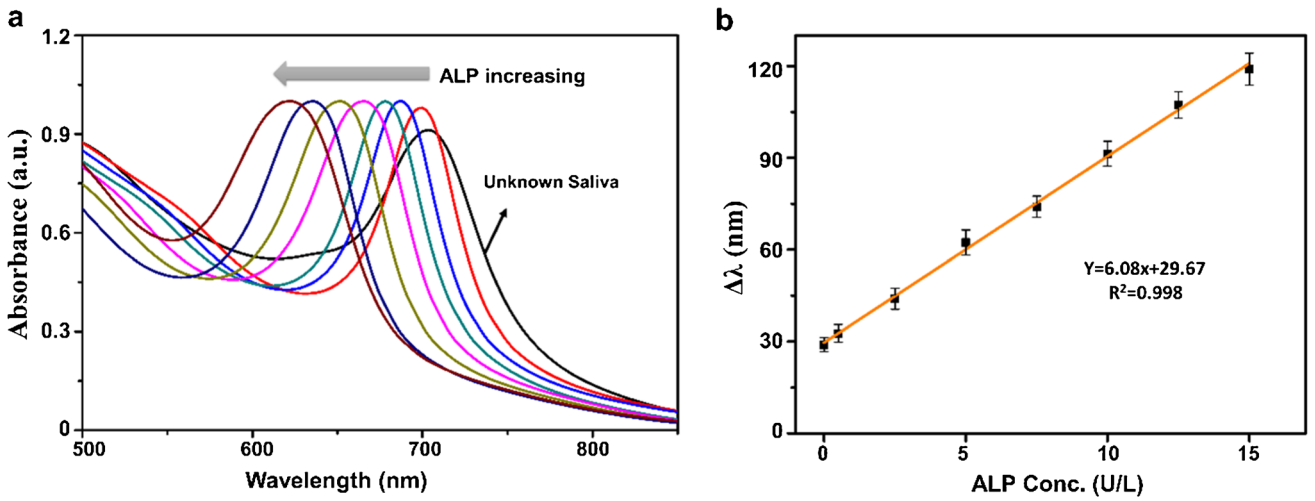

Fig. 6 (**a**) UV–Vis spectra of the multicolor ALP biosensor with different amounts of added ALP in a 10% diluted saliva solution and (**b**) linear standard addition calibration curve of the change in absorbance of the multicolor biosensor as a function of the added ALP concentration

Table 2 Analytical results of the ALP assay in the 10% diluted saliva solution using the standard addition method

Sample	Added (U/L)	Total expected (U/L)	Detected (U/L)	Recoveries (%)	RSD (%)
Saliva (10% diluted)	0	4.67	4.67	-	-
	0.5	5.17	5.045	98.1	4.40
	3	7.67	7.469	97.5	3.91
	5	9.67	9.69	100.3	4.75

Conclusions

ALP is a versatile biomarker for monitoring not only human metabolism but also several diseases, such as periodontitis and oral carcinoma. We successfully developed a multicolor biosensor for ALP assay based on the simultaneous modification of both composition and morphology of AuNBPs. The bioassay is based on the selective catalytic activity of the ALP to dephosphorylate glucose phosphate substrate into glucose, thus reducing Ag ions into Ag nanoshells on the surface of AuNBPs. We successfully provided a binary surfactant mixture comprising CTAB and Tween 20, which provided maximum blue shift of LSPR with multicolor response of high color resolution as functional of the ALP concentration. The used binary surfactant promoted a uniform growth of the Ag on the surface of AuNBPs. The controlled growth of Ag leads to distinctive color change as functional of ALP concentration. The spectral changes exhibited a high sensitivity to ALP detection, enabling us to achieve the low limit of detection (0.085 U/L). Furthermore, the high selectivity and high reliability of the developed multicolor ALP biosensor were successfully demonstrated through an interference test and a standard addition method, respectively, proving the suitability of the developed biosensor for daily applications.

Supplementary Information The online version contains supplementary material available at https://doi.org/10.1007/s00604-021-05080-w.

Funding This research was supported in part by the National Research Foundation of Korea (No. 2021M3H4A1A02056037) and the National Research Foundation of Korea(NRF) grant funded by the Korea government(MSIT) (No.2020R1A5A1018052).

Declarations

Competing interests The authors declare no competing interests.

References

1. Malathi N, Mythili S, Vasanthi HR (2014) Salivary diagnostics: a brief review. ISRN Dent 2014:158786
2. Kinney JS, Ramseier CA, Giannobile WV (2007) Oral fluid-based biomarkers of alveolar bone loss in periodontitis. Ann N Y Acad Sci 1098:230–251
3. Nakamura M, Slots J (1983) Salivary enzymes. J Periodontal Res 18(6):559–569
4. Dabra S, Singh P (2012) Evaluating the levels of salivary alkaline and acid phosphatase activities as biochemical markers for periodontal disease: a case series. Dent Res J (Isfahan) 9(1):41–45
5. Shi D et al (2016) Naked-eye sensitive detection of alkaline phosphatase (ALP) and pyrophosphate (PPi) based on a horseradish peroxidase catalytic colorimetric system with Cu(II). Analyst 141(19):5549–5554
6. Hu Q et al (2017) Sensitive and selective colorimetric assay of alkaline phosphatase activity with Cu(II)-phenanthroline complex. Talanta 163:146–152
7. Hu Q et al (2017) Facile colorimetric assay of alkaline phosphatase activity using Fe(II)-phenanthroline reporter. Anal Chim Acta 950:170–177
8. Zhang Z et al (2015) Iodine-mediated etching of gold nanorods for plasmonic ELISA based on colorimetric detection of alkaline phosphatase. ACS Appl Mater Interfaces 7(50):27639–27645
9. Rojas-Avelizapa NG, Gómez-Ramírez M, Hernández-Gama R, Aburto J, García de León R (2013) Isolation and selection of sulfur-oxidizing bacteria for the treatment of sulfur-containing hazardous wastes. Chem Biochem Eng Q 27(1):109–117
10. Ye K et al (2019) Bifunctional MIL-53(Fe) with pyrophosphate-mediated peroxidase-like activity and oxidation-stimulated fluorescence switching for alkaline phosphatase detection. J Mater Chem B 7(31):4794–4800
11. Li PF et al (2017) A fluorescent probe for pyrophosphate based on tetraphenylethylene derivative with aggregation-induced emission characteristics. ChemistrySelect 2(13):3788–3793
12. Wang F et al (2017) Label-free upconversion nanoparticles-based fluorescent probes for sequential sensing of Cu2+, pyrophosphate and alkaline phosphatase activity. Biosens Bioelectron 95:21–26
13. Liu H et al (2017) A turn-on fluorescent sensor for selective and sensitive detection of alkaline phosphatase activity with gold nanoclusters based on inner filter effect. ACS Appl Mater Interfaces 9(1):120–126
14. Ruan C, Wang W, Gu B (2006) Detection of alkaline phosphatase using surface-enhanced raman spectroscopy. Anal Chem 78(10):3379–3384
15. Ingram AM, Moore BD, Graham D (2009) Simultaneous detection of alkaline phosphatase and beta-galactosidase activity using SERRS. Bioorg Med Chem Lett 19:1569–1571
16. Sun D et al (2019) Cellular heterogeneity identified by single-cell alkaline phosphatase (ALP) via a SERRS-microfluidic droplet platform. Lab Chip 19(2):335–342
17. Zeng Y et al (2017) Rapid and reliable detection of alkaline phosphatase by a hot spots amplification strategy based on well-controlled assembly on single nanoparticle. ACS Appl Mater Interfaces 9(35):29547–29553
18. Craig DB, Wong JCY, Dovichi NJ (1996) Detection of attomolar concentrations of alkaline phosphatase by capillary electrophoresis using laser-induced fluorescence detection. Anal Chem 68(4):697–700
19. Wu D, Regnier FE, Linhares MC (1994) Electrophoretically mediated micro-assay of alkaline phosphatase using electrochemical and spectrophotometric detection in capillary electrophoresis. J Chromatogr B Biomed Appl 657(2):357–363
20. Whisnant AR, Johnston SE, Gilman SD (2000) Capillary electrophoretic analysis of alkaline phosphatase inhibition by theophylline. Electrophoresis 21(7):1341–1348
21. Ino K et al (2012) Novel electrochemical methodology for activity estimation of alkaline phosphatase based on solubility difference. Anal Chem 84(18):7593–7598
22. Peng J et al (2015) Copper sulfide nanoparticle-decorated graphene as a catalytic amplification platform for electrochemical detection of alkaline phosphatase activity. Anal Chim Acta 878:87–94
23. Wu Z et al (2016) Reliable digital single molecule electrochemistry for ultrasensitive alkaline phosphatase detection. Anal Chem 88(18):9166–9172
24. Mayer KM, Hafner JH (2011) Localized surface plasmon resonance sensors. Chem Rev 111(6):3828–3857

25. Min Y, Wang Y (2020) Manipulating bimetallic nanostructures with tunable localized surface plasmon resonance and their applications for sensing. Front Chem 8:411
26. Breslow R, Katz I (1968) Relative reactivities of p-nitrophenyl phosphate and phosphorothioate toward alkaline phosphatase and in aqueous hydrolysis. J Am Chem Soc 90(26):7376–7377
27. Bowers GN Jr, McComb RB (1966) A continuous spectrophotometric method for measuring the activity of serum alkaline phosphatase. Clin Chem 12(2):70–89
28. Grap MJ et al (2015) Use of high frequency ultrasound to detect changes in skin integrity: an image evaluation validation procedure. Intensive Crit Care Nurs 31(3):141–147
29. Xu S et al (2017) Highly uniform gold nanobipyramids for ultrasensitive colorimetric detection of influenza virus. Anal Chem 89(3):1617–1623
30. Song H et al (2018) Sensitive and selective colorimetric detection of alkaline phosphatase activity based on phosphate anion-quenched oxidase-mimicking activity of Ce(IV) ions. Anal Chim Acta 1044:154–161
31. Wang X, Jiang X, Wei H (2020) Phosphate-responsive 2D-metal-organic-framework-nanozymes for colorimetric detection of alkaline phosphatase. J Mater Chem B 8(31):6905–6911
32. Liu Y et al (2019) Plasmonic and photothermal immunoassay via enzyme-triggered crystal growth on gold nanostars. Anal Chem 91(3):2086–2092
33. Gao J et al (2018) Prereduction-promoted enhanced growth of silver nanoparticles for ultrasensitive colorimetric detection of alkaline phosphatase and carbohydrate antigen 125. Talanta 189:129–136
34. Luo M et al (2020) Simply converting color signal readout into thermal signal readout for breaking the color resolution limitation of colorimetric sensor. Sens Actuators B Chem 309:127707
35. Tang Y et al (2017) Competitive photometric and visual ELISA for aflatoxin B1 based on the inhibition of the oxidation of ABTS. Microchim Acta 184(7):2387–2394
36. Yan X et al (2019) Fluorescent detection of ascorbic acid using glutathione stabilized Au nanoclusters. Chem Phys 522:211–213
37. May BMM, Parani S, Oluwafemi OS (2019) Detection of ascorbic acid using green synthesized AgInS2 quantum dots. Mater Lett 236:432–435
38. Dhara K, Debiprosad RM (2019) Review on nanomaterials-enabled electrochemical sensors for ascorbic acid detection. Anal Biochem 586:113415
39. Kong L et al (2020) A novel smartphone-based CD-spectrometer for high sensitive and cost-effective colorimetric detection of ascorbic acid. Anal Chim Acta 1093:150–159
40. Guo Z et al (2012) High-purity gold nanobipyramids can be obtained by an electrolyte-assisted and functionalization-free separation route. Colloids Surf A Physicochem Eng Asp 414:492–497
41. Li Q et al (2015) Production of monodisperse gold nanobipyramids with number percentages approaching 100% and evaluation of their plasmonic properties. Adv Opt Mater 3(6):801–812
42. Zhu X et al (2016) Gold nanobipyramid-supported silver nanostructures with narrow plasmon linewidths and improved chemical stability. Adv Func Mater 26(3):341–352
43. Li Q et al (2012) Crystalline structure-dependent growth of bimetallic nanostructures. Nanoscale 4(22):7070–7077
44. Huang C-C, Yang Z, Chang H-T (2004) Synthesis of dumbbell-shaped Au−Ag core−shell nanorods by seed-mediated growth under alkaline conditions. Langmuir 20(15):6089–6092
45. Liu, Guyot-Sionnest P (2004) Synthesis and optical characterization of Au/Ag core/shell nanorods. J Phys Chem B 108(19):5882–5888
46. Ah CS, Hong SD, Jang D-J (2001) Preparation of AucoreAgshell nanorods and characterization of their surface plasmon resonances. J Phys Chem B 105(33):7871–7873
47. Gao Z et al (2014) High-resolution colorimetric assay for rapid visual readout of phosphatase activity based on gold/silver core/shell nanorod. ACS Appl Mater Interfaces 6(20):18243–18250
48. Wang C et al (2018) Colorimetric logic gate for alkaline phosphatase based on copper (II)-based metal-organic frameworks with peroxidase-like activity. Anal Chim Acta 1004:74–81
49. Tang C et al (2016) A fluorometric assay for alkaline phosphatase activity based on β-cyclodextrin-modified carbon quantum dots through host-guest recognition. Biosens Bioelectron 83:274–280
50. Sun J et al (2016) Fluorescence immunoassay system via enzyme-enabled in situ synthesis of fluorescent silicon nanoparticles. Anal Chem 88(19):9789–9795
51. Qian Z et al (2015) Carbon quantum dots-based recyclable real-time fluorescence assay for alkaline phosphatase with adenosine triphosphate as substrate. Anal Chem 87(5):2966–2973
52. Song Z et al (2014) A ratiometric fluorescent probe based on ESIPT and AIE processes for alkaline phosphatase activity assay and visualization in living cells. ACS Appl Mater Interfaces 6(19):17245–17254
53. Malashikhina N, Garai-Ibabe G, Pavlov V (2013) Unconventional application of conventional enzymatic substrate: first fluorogenic immunoassay based on enzymatic formation of quantum dots. Anal Chem 85(14):6866–6870
54. Jiang H, Wang X (2012) Alkaline phosphatase-responsive anodic electrochemiluminescence of CdSe nanoparticles. Anal Chem 84(16):6986–6993

Publisher's note Springer Nature remains neutral with regard to jurisdictional claims in published maps and institutional affiliations.